A Reproducible, Multimodal, Triple-Network Neurobiology of Depressive Rumination

Pisner, D.A., Shumake, J., Beevers, C.G., Schnyer, D.M.
Department of Psychology and Institute for Mental Health Research
University of Texas at Austin

Abstract

Functional brain networks including Default Mode, Salience, and Executive Control (DMN; SN; ECN), collectively called the 'triple-network', are associated with Depressive Rumination (DR) severity in Major Depressive Disorder (MDD). The underlying white-matter (WM) microstructure supporting these networks and its precise role in DR remains unknown, however. Using diffusion MRI and resting-state BOLD fMRI, we explored multimodal relationships between DR, WM microstructure, and triple-network functional connectivity in adults with MDD ($N = 39$), and then replicated our analyses in an independent dataset of adults with MDD ($N = 39$). Results showed that higher DR severity was negatively associated with: (a) microstructure of primary and secondary WM fibers spanning the right Superior Longitudinal Fasciculus and surrounding clusters, (b) functional network connectivity of the Cingulo-Opercular SN (coSN), Precuneal DMN (pDMN), and frontal ECN (fECN), (c) inverse correlations between the pDMN and each of the coSN and fECN, and (d) a direct correlation between the fECN and coSN. Ultimately, thirty-one findings replicated fully or partially, lending support to the conclusion that individual differences in WM microstructure, resting-state functional connectivity of the triple-network, and their multivariate, microstructural-functional intersection, provide a neurobiological basis for depressive rumination.

Keywords:

Multimodal, Microstructure, Resting-State, Triple-Network, Rumination, Replication

Cognitive models of depression posit that negatively biased self-referential processing plays a critical role in maintaining the disorder[1]. Depressive Rumination (DR) is the *perseverative* form of this cognitive bias that involves a repetitive focus on "one's depressive symptoms and on the implications of those symptoms"[2]. In Major Depressive Disorder (MDD), DR significantly contributes to depressive symptom severity[2], duration[3], and relapse likelihood[4]. Despite its clear role in MDD maintenance, few effective treatments for DR have been developed[5,6]. By delineating reproducible neurobiological models of DR, researchers could identify more precise treatment targets, potentially spurring development of more effective neurocognitive interventions for MDD[7,8].

Structural and Functional Modular Models of Depressive Rumination

At the core of DR is self-referential processing[9], which is inwardly-directed attention focused on the self. This mechanism has been associated with functional activation of grey matter cortices such as the Anterior Cingulate (ACC), Posterior Cingulate (PCC)[10], and the Precuneus[11], each of which processes some form of information about the self[12]. Although few studies have explored grey matter structural biomarkers of DR, one study found reduced grey matter volume of the right superior Temporal Gyrus[13], which contains the Auditory Cortex and is essential for language processing, but may also be critical for 'insight' problem-solving[14].

Emotional salience, a second proposed mechanism of DR, may be further necessary for assigning a negative bias to self-referential processing. A wealth of literature has shown that emotional salience is associated with both brain function and structure of the Amygdala, Insula, and Anterior Cingulate Cortex (ACC), among other regions. Greater sustained activation within the Amygdala has been observed, for example, in response to negative-valence words following non-emotional words among depressed individuals[15]. Another study found that when controlling for Amygdala activity, the anterior Insula explained nearly 10% of variance in DR severity[16]. Oher experiments have shown that the ACC could also play a variety of roles in DR, but findings have been mixed[9,17,18]. On the one hand, this may reflect the variety of motivational states that are engaged by different task paradigms[19], but it could also reflect the multiple specialized functions among sub-regions of the ACC itself[20] or its dense interconnectivity with other cortical areas[21].

A third proposed mechanism of DR is disrupted top-down cognitive control, which may instantiate repeated failures to disengage from negatively-salient self-referential processing, thereby impairing attentional shifts towards neutral or positive thoughts[22]. In depressed

individuals, this 'impaired disengagement'[23] is thought to amplify and sustain the negative bias of self-referential processing by spurring a vicious cycle of self-criticism that drains cognitive resources needed to counteract the increase[24]. Thus, disrupted cognitive control is often believed to underlie the perseverative nature of DR that distinguishes it from more adaptive, reflective forms of rumination[4,25]. Broadly construed, disrupted cognitive control in DR likely implicates aberrant structural and functional properties of cognitive control modules like the dorsolateral and inferior Prefrontal Cortices[17,26,27], whose activation patterns are largely titrated by the ACC[21].

Structural and Functional Connectivity Models of Depressive Rumination

Although studies of modular biomarkers have identified a core set of nodes relevant to each of the three proposed mechanisms of DR, the modular perspective fails to account for dynamic interactions among those nodes[28]. Modular biomarkers of disrupted cognitive control may exhibit a variety of functional configurations across brain hemispheres and in relation to one another, for instance, depending on the nature of the stimulus and task paradigm used[29]. To capture more precise brain-cognition relationships relevant to DR, recent directions have instead begun to elucidate connectivity biomarkers across both functional[30,31] and structural[32] modalities.

Studies of structural connectivity typically employ diffusion tensor MRI (dMRI), which provides an in vivo method for measuring the global and local microstructure of known white matter (WM) pathways between grey matter modules that collectively form a brain network[33]. Using Tract-Based Spatial Statistics (TBSS) applied to dMRI, one study[32] examined Fractional Anisotropy (FA), a proximal measure of WM microstructural connectivity, to show that the left Superior Longitudinal Fasciculus (SLF) and neighboring motor fibers were strongly associated with DR ($p<0.05$, Bonferroni corrected).[32] Due to its small sample size ($n=16$), however, the results of that study may not generalize to other depressed populations[58].

There are many more studies of functional connectivity in DR. Those employing resting-state functional MRI (rsfMRI) have especially attracted interest, perhaps since rumination is believed to operate predominantly in a task-negative brain state[36]. Three resting state networks (RSN's) in particular, corresponding to each of the three proposed mechanisms of DR, have permeated the rsfMRI research of DR—the Default Mode, Salience, and Executive Control networks (DMN; SN; ECN)[24,30]. Despite their diversity of specialized intrinsic functions, they themselves are also known to interact[37] and have therefore further been described as belonging to

a mesoscale system of networks, dubbed the 'triple-network', whose broad disruption may be found across multiple forms of psychopathology, including MDD[37].

The DMN appears to play a critical role in self-referential processing in DR, likely by coordinating the brain's core autobiographical memory modules[38,39]. On the other hand, reduced DMN activity during externally-focused attention is believed to attenuate self-referential processing so as to direct cognitive resources more efficiently[39]. Perhaps most notably, lower functional connectivity within the parietal sub-system of the DMN has been repeatedly shown to predict greater rumination severity in MDD[36].

In contrast, a recent study of depressed teenagers highlighted a critical role for the SN as sub-serving negative cognitive bias and self-criticism in DR[57]. One reason for this association may be that aberrant functional connectivity of the SN during self-referential processing could result in poor coordination of dopaminergic signaling[40] and misappropriated 'tagging' of self-relevant thoughts with negative bias[9]. Along these lines, a recent task-based fMRI study showed that depressed ruminators tend to more actively recruit SN nodes simultaneously during reward anticipation, suggesting a role for elevated affective sensitivity to self-relevant cues in DR[41]. Since the SN also coordinates attention shifting of the triple-network as a whole[42], aberrant SN functional connectivity patterns associated with DR might also reflect disrupted switching between the DMN and ECN[43].

Unlike the DMN and SN, whose associations with DR are perhaps primarily related to *intrinsic* functional connectivity patterns (i.e. including only those nodes belonging to the respective networks)[9,30], the ECN's role in DR may further involve *extrinsic* functional connectivity patterns (i.e. with modules or other RSN's outside of that network). The ECN has been shown to interact with modular limbic regions like the Amygdala[44], for instance, but also with each of the SN and DMN as a whole[45]. In fact, one study showed that depression-remitted youth who exhibit higher ECN-DMN extrinsic functional connectivity may have a greater ability to downregulate self-referential thought[46]. Another study similarly demonstrated that higher DMN dominance with lower ECN engagement, especially when accompanied by higher Insula activity, predicted higher DR severity[45].

Towards a systems level understanding of depressive rumination

In summary, DR's neurobiology is likely characterized by a variety of structural and functional biomarkers, operating across multiple levels of neural complexity, that correspond to

at least three proposed cognitive mechanisms of DR. This apparently diverse pathophysiology suggests that a *joint microstructural-functional network connectivity* perspective might greatly enhance scientific understanding of DR. Indeed, recent studies outside of rumination literature have shown that microstructural connectivity of fronto-parietal tracts such as the Cingulum and Uncinate Fasciculus (UF) may support the DMN[47] and ECN[48], respectively. Hence, neuroscientific appeals made to either structural or functional connectivity biomarkers of DR, considered in isolation, could conversely reduce the precision of our etiological understanding[49]. Thus, multimodal studies are needed to clarify potential systems-level[50] interactions between microstructural and functional brain connectivity amongst individuals prone to DR[32].

Our hypotheses are two-fold: 1) a shared neurobiology of DR exists and implicates both microstructural and 'triple-network' functional connectivity, corresponding to three proposed cognitive mechanisms of DR that include aberrant self-referential processing, negatively-biased salience processing, and disrupted cognitive control; 2) individual differences in DR severity need be explained cross-modally, through joint appeal to triple-network functional connectivity with respect to underlying microstructural connectivity constraints.

To test and explore these hypotheses, we utilize data from two neuroimaging modalities, dMRI and rsfMRI. Given the present state of replication crisis in neuroscience[51] and the growing need for more credible and reproducible neurobiological models of disordered cognition[52], data were obtained from two separate datasets. This approach allowed us to determine whether initial findings could be directly replicated in a second, independent sample. Our analyses test the first hypothesis applying multiple linear regression analyses to the dMRI and rsfMRI data to explore various microstructural and functional connectivity associations with DR, respectively. The dMRI analyses include TBSS and global probabilistic tractography[33], whereas the rsfMRI analyses include ICA-based examinations of both intrinsic and extrinsic resting-state functional connectivity[30]. We then test the second hypothesis by jointly examining microstructural-functional connectivity relationships associated with DR. Lastly, we re-test both of our hypotheses and each of their associated statistical tests by applying our exact analytic pipeline developed for the initial dataset to an independent dataset made publicly available from NKI Rockland[53,54].

METHODS

Participants: Initial Sample

Thirty-nine treatment-seeking participants with DSM-IV Major Depressive Disorder (MDD) were recruited for this study from advertisements placed online, in newspapers, and on late night TV. Participants were screened for medical or physical conditions that would preclude participation in an MRI study. They also completed an abbreviated Mini International Neuropsychiatric Interview (MINI)[55] to determine provisional MDD diagnosis, which were then confirmed using in-person Structured Clinical Interviews for the DSM-IV Disorders (SCID)[56] administered by a trained research assistant. Participants were excluded if they met criteria for past year substance abuse or dependence, current or past psychotic disorder, bipolar disorder, and schizophrenia. Participants receiving pharmacological treatment were allowed into the study if there has been no medication change in the 12 weeks prior to study entry. To minimize brain changes associated with aging, individuals were between the age of 18 and 55[57].

Ethics Statement

The Institutional Review Board at the University of Texas at Austin approved all study procedures and materials and all participants provided signed informed consent.

Depressive Rumination Measurement

The RSQ (Response Styles Questionnaire)[58] is a 10-item self-report measure of the tendency to ruminate. It consists of a total score and two sub-scales: reflection and brooding. The reflection subscale measures an individual's tendency to turn inward to engage in problem-solving and thereby alleviate negative or depressed mood[4], whereas brooding measures the maladaptive form of rumination believed to be a proxy for DR[4,45]. Brooding specifically reflects the intensity of ruminative responses to expressions of negative emotion[2]. The brooding subscale has high reliability (α=0.77-0.92)[58], is well-validated within depressed populations[59], decontaminated of any explicitly depressive content[59], and the sub-scale of choice for most neurobiological studies of DR[9,22,30,36,45]. For these reasons, we used the brooding subscale exclusively to measure DR.

Imaging Acquisition

MRI scans were acquired on a whole body 3T GE MRI with an 8-channel phase array head coil. The scanning protocol involved collection of a localizer followed by a high-resolution T1 structural scan, two resting state scans of 6 minutes each, a second high-resolution structural

scan, and finally a 55-direction diffusion tensor (dMRI) scan. For the resting-state scan, instructions were presented utilizing a back-projection screen located in the MR bore and viewed through a mirror mounted on the top of the head coil. Participants were instructed to remain awake and alert and keep their gaze on a fixation cross (+) presented approximately at the center of their field of view for the 6-minute duration of the scan. (*See* Appendices, Methods**: Section A***)*.

dMRI Preprocessing

Preprocessing of Diffusion Magnetic Resonance Imaging (dMRI) data was carried out using a custom preprocessing workflow that included eddy correction, brain extraction, denoising, and tensor/ball-and-stick model fitting tools adapted from the FMRIB Diffusion Toolbox[60]. To achieve maximal sensitivity and specificity from the dMRI data, preprocessing included rigorous automated and manual quality control steps (*see* Appendices, Methods: **B)**.

dMRI: Structural Connectivity and DR

A number of approaches to dMRI analysis were implemented. To begin, the whole-brain was interrogated using Tract-Based Spatial Statistics (TBSS)[61] to identify microstructural characteristics that were associated with brooding severity (*see* Appendices, Methods: **Section C**). We additionally employed the 'crossing-fibers' extension of TBSS[62], which is less often used due to its computational expense, but can uniquely capture group differences in crossing fibers, unlike TBSS based on the tensor model alone.

For statistical testing, a permutation approach was employed using FSL's "randomise" function with the TFCE Threshold-Free Cluster Enhancement option, generating 10,000 permutations and applying family-wise error (FWE)-correction to obtain cluster inferences. A two-tailed regression model was next generated using FSL's GLM function, whereby RSQ brooding scores were used as the criterion variable with age and gender as nuisance covariates. Age was included due to a well-known confounding influence of age on WM microstructure[63], and gender was included initially due to some evidence of gender differences in rumination—namely, that females tend to ruminate more than males[64]. The resulting negative contrast mask was thresholded twice—first at p=0.05 and again at p=0.01.

Following TBSS, we sought to corroborate our initial group level, voxel-wise dMRI findings using individual level tractography, which is an alternative dMRI methodology that attempts to reconstruct known WM pathways while retaining each subject's image in native

space orientation. Since spatial information is not manipulated in tractgoraphy as it is with TBSS[65], tractography could confirm any TBSS findings in native space, while also disconfirm false-positives due to non-physiological factors such as image misalignment, movement, and other factors resulting from the methodological limitations of TBSS[66].

For tractography, we chose to analyze average FA measures from the entire pathways of tracts of interest whose labels included significant voxels from the earlier TBSS stage. These measures were then further analyzed across hemispheres to establish any significant laterality effects[67]. To perform tractography, we specifically used the TRActs Constrained by UnderLying Anatomy (TRACULA) tool in FreeSurfer (version 5.3.0)[33], which delineates 18 known WM bundles using each participant's joint dMRI and T1 weighted MRI data (*See* Appendices, Methods: **Section D**).

rsfMRI Preprocessing

Preprocessing of baseline rsfMRI data was carried out using a custom workflow based on FSL's FEAT[60], combined with AFNI and FREESURFER tools. Additional denoising steps were taken by controlling for WM and ventricular CSF confounds, and by using FSL's ICA-based Xnoisifier artifact removal tool (FIX) to control for motion and physiological artifact (*See* Appendices, Methods: **Section E**).

rsfMRI: Group-ICA / Dual-regression and Depressive Rumination

Group-level Independent Components Analysis (ICA) was performed by employing "temporal concatenation" of the complete, preprocessed rsfMRI time-series from all of the participants and restricted to twenty-five independent component (IC) outputs[68]. Four IC's were manually identified as noise and removed from further examination. Of the remaining twenty-one networks, all were identified using visual inspection by way of reference to the 17 RSN's delineated by the Yeo et al. 2011 atlas[69], thus allowing for identification of the three IC's of the triple-network that were introduced above - the pDMN[36,45], the coSN[70], and the fECN[24,71,72].

A dual-regression approach[73] was next performed on the triple-network RSN's, which were used as regressors for each individual subject's 4D set of fMRI volumes in order to extract time-series that were both specific to each subject and specific to each of the three IC's[64]. Design matrices and contrasts were then created to test for correlations between brooding severity and total average intrinsic connectivity within each of these RSN's, controlling for age and gender. These regression models were tested separately for each RSN, using two-tailed contrasts in an

identical manner to that used in TBSS, with FSL's randomise (10,000 permutations) and TFCE cluster-thresholding with whole-brain FWE-correction[74]. To further correct for analysis-level multiple comparisons (i.e. to account for the testing of three different RSN's), we also Bonferroni-corrected our *p*-value significance thresholds for these models to p=0.02.

Between-Network Functional Connectivity

To investigate interactions between the triple-network RSN's, we utilized FSLNets[75], a MATLAB-based tool that interfaces with FSL. FSLNets utilizes the individual resting-state network IC's generated from the earlier dual-regression stage to perform hierarchical clustering across RSN's and estimate a partial-correlation (Spearman's ρ) matrix for each RSN for each participant.

To perform cross-subject, between-RSN general linear modeling, randomise was again employed, but this time using the nets_glm function at 10,000 permutations. The design matrices and contrasts used in the earlier FSL GLM analyses, were again used in this analysis. Subsequently, the between-network partial correlation coefficients were extracted as a 1D vector of average total connectivity values for each of the triple-network IC's so as to further conduct exploratory analyses in R 3.3.1.

In summary, whereas the dual-regression approach identified DR-associated clusters (both *belonging to* and *external to* the RSN's) that are more strongly connected to each of the triple-network RSN's considered separately, the FSLnets approach identified DR-associated patterns of between-network correlation among the triple-network RSN's considered collectively.

Replication

To address whether the findings would generalize beyond the initial sample[54], we replicated all stages of analysis using an independent dataset with identical data types and handling, and then explored whether we obtained equivalent and/or comparable findings. To realize this aim, we obtained access to the publicly-available, multi-site NKI Rockland dataset[53], which contained a sub-sample of participants with equivalent demographics and measures to those participants from our original sample; this included (n=39) participants who met criteria for some form of depressive disorder (MDD, persistent/recurrent depression, or dysphoria), were between the ages of 18-55, had no history of drug abuse or severe comorbid psychopathology, and had useable MRI data (*See* Appendices, Methods: **Sections F & G**). Participants were

administered the 22-item Rumination Response Scale (RRS)(*See* METHODS: **Depressive Rumination Measurement**), which contained identical brooding sub-scale items to those administered in the 10-item RSQ scale[59].

RESULTS: INITIAL SAMPLE

Descriptive Statistics and Behavioral Findings

Depressive rumination severity (DR) was normally distributed (M= 9.08, SD= 3.01, IQR=5; Shapiro-Wilk = 0.976, p = 0.528) and modestly associated with depression severity (R^2 = 0.13, $F(1, 37) = 5.61$, p=0.02). Age was positively skewed (M=27.51, SD = 8.80) due to an overrepresentation of young adults in our initial sample. Both age and gender were included as nuisance covariates in the initial TBSS and dual-regression analysis due to their potential for confounding the neuroimaging analyses (*see* METHODS**: Sample Characteristics**) and because of a weak correlation between age and RSQ brooding scores (R^2 = 0.09, $F(1, 37) = 3.84$, p<0.06). Once gender was definitively determined to be a non-confounding factor in our sample from these initial analyses, however, only age was retained as a nuisance covariate for all subsequent analyses.

White Matter Microstructure and Depressive Rumination

TBSS Findings

Our first set of analyses employed tensor and crossing-fiber variations of TBSS to test for WM microstructural connectivity biomarkers of DR (*see* METHODS: **TBSS;** Appendices, Methods: **Section C**). Results first revealed significantly lower FA in association with higher brooding scores within the right Superior Longitudinal Fasciculus (SLF, both parietal and particularly temporal parts), the complete body of the Cingulum, and the right and left Corticospinal Tract (CST) (p<0.01 FWE; p<0.05 FWE; *see* **Figure 1**). Some of these voxels also extended into the Anterior Thalamic Radiation (ATR), Uncinate Fasciculus (UF), and Splenium (p<0.05 FWE; p<0.05 FWE; p<0.05 FWE). A subsequent 'crossing-fibers' TBSS analysis closely tracked these findings, but further revealed significant relationships between DR and the integrity of crossing-fibers (captured by the F2 partial volume) in a small cluster of the right anterior Corona Radiata where the SLFT intersects with the Corpus Callosum at the Centrum Semiovale (p<0.01 FWE; *see* **Figure 1***)*.

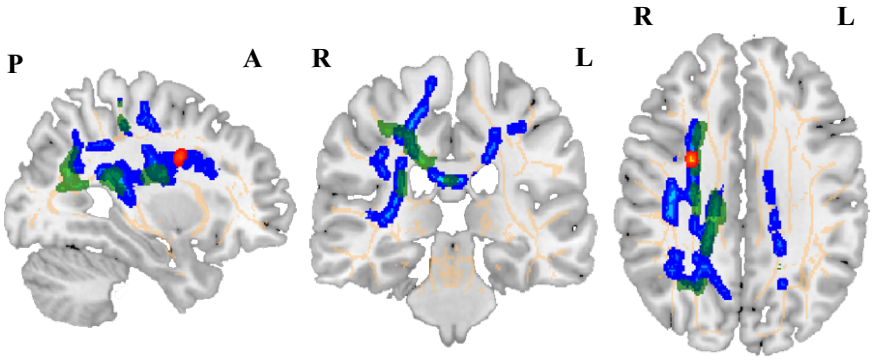

Figure 1: Depressive rumination was associated WM integrity primarily within the temporal and parietal parts of the right SLF including the anterior and posterior Corona Radiata, as well as the right posterior and anterior Cingulum along with the bilateral CST, particularly near its intersection with the posterior Corona Radiata. Here, significant associations with FA ($p<0.01$) are depicted in blue, significant associations with the F1 partial volume ($p<0.01$) are depicted in green, and significant associations with the F2 "crossing-fibers" volume at the Centrum Semiovale of the anterior Corona Radiata ($p<0.01$) are depicted in red-yellow.

Tractography Findings

Using global probabilistic tractography, we next sought to methodologically triangulate and anatomically clarify the TBSS findings by exploring each major fiber bundle separately[33]. Using six pathways of interest from the outputs of TRACULA including the SLFT (Temporal part), SLFP (Parietal part), CCG, CST, ATR, and Splenium, we found that average FA of the right SLFT, right SLFP, right CCG, and CST negatively predicted brooding severity. This supported the findings conducted on a voxel-wise basis with TBSS, and suggested that DR may be primarily associated with these four tracts globally, despite the presence of isolated 'local' WM clusters associated with DR beyond these pathways. Although the strength of the negative associations between brooding scores and average FA of the right CCG ($R^2 = 0.10$, $F(2, 36) = 2.05$, $p=0.08$) and CST ($R^2 = 0.12$, $F(2, 36) = 2.44$, $p=0.05$) was small, the association between DR and average FA of the right SLFP was moderate ($R^2 = 0.15$, $F(2, 36) = 3.14$, $p < 0.05$), and the association between DR and average FA of the right SLFT survived Bonferroni Correction ($R^2 = 0.25$, $F(2, 36) = 5.92$, $p=0.002$).

Hemisphericity

With the exception of the bilateral CST, the WM findings were predominantly right-lateralized. To show this, we treated hemisphere as a within-subjects measure and used Analysis of Variance (ANOVA) to compare two GLM's predicting brooding scores for each tractography measure of average FA. Specifically, the first GLM used left hemisphere as the predictor,

whereas the second GLM used right hemisphere as the predictor, controlling for left hemisphere. Ultimately, we found that the effect of hemisphere was significant for both the right SLFT ($p<0.01$) and right SLFP ($p<0.05$), which exhibited a stronger relationship with brooding scores than did their contralateral counterparts (*See Appendices, Results* **Section A**).

<u>'Within-Network' Functional Connectivity and Depressive Rumination</u>

Dual-Regression Findings

We next tested whether DR was associated with resting-state functional connectivity of the three triple-network RSN's as identified from the outputs of group-ICA followed by dual-regression (*see* METHODS: **rsfMRI Group-ICA** & **Dual-regression**), and additionally, whether the DR-associated WM microstructure measures might predict these functional connectivity measures. Results revealed that DR was strongly correlated with functional connectivity with multiple clusters, some of which belonged to each respective triple-network RSN (i.e. 'intrinsic' connectivity), but some of which were outside of the respective RSN's (i.e. 'extrinsic' connectivity) (*see* **Figure 2**). With respect to the latter, we found that extrinsic connectivity of the right dorsolateral prefrontal cortex of the frontal Executive Control Network (fECN) with a small cluster (voxels=15) at a juncture between the left Amygdala and Parahippocampal Gyrus was positively associated with brooding scores ($p<0.05$ FWE**;** *see blue clusters in* **Figure 2**). Additionally, the Precuneal Default Mode Network (pDMN) exhibited lower extrinsic connectivity with the left somatosensory areas, left Precentral Gyrus and left inferior Frontal Gyrus ($p<0.01$ FWE; *see red clusters in* **Figure 2**), but also lower intrinsic functional connectivity, specifically between clusters of the right Precuneus and PCC. Lastly, the Cingulo-Opercular Salience Network (coSN) exhibited lower intrinsic connectivity within several clusters of the left Precentral Gyrus, left inferior Frontal Gyrus, and left and right anterior Insula ($p<0.01$ FWE ; *see green clusters in* **Figure 2**).

WM Microstructure and 'Within-Network' Functional Connectivity

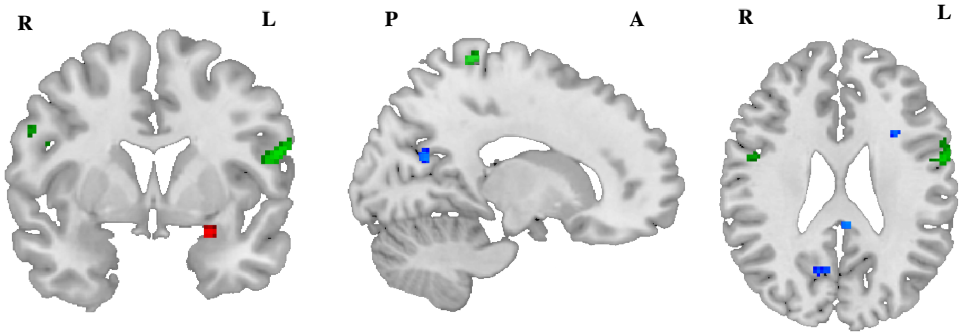

Figure 2: Significant clusters exhibiting lower functional connectivity within the pDMN associated with DR are depicted in blue, and include the PCC, Precuneus, left Precentral Gyrus, left Somatosensory Cortex, and the left inferior Frontal Gyrus. Significant clusters exhibiting lower functional connectivity within the coSN are depicted in green and include the left Precentral Gyrus, right superior Postcentral gyrus, and bilateral clusters of the inferior Frontal Gyrus and anterior Insula highlighted. Finally, significant clusters exhibiting greater functional connectivity within the fECN are depicted in red and include the left Amygdala and left Parahippocampal Gyrus.

We next extracted the average total connectivity beta coefficients for each of the significant dual-regression clusters from the pDMN, coSN, and fECN associated with DR so that we could test for relationships between the functional connectivity findings (i.e. informed by dual-regression) and the microstructural connectivity findings (i.e. informed by tractography and TBSS). This required creating a matched subsample of n=32 subjects, since seven subjects did not have both useable rsfMRI and TRACULA data.

Tractography showed that average FA of the right SLFT, and to a lesser extent the SLFP, was positively associated total average intrinsic connectivity of the coSN ($R^2 = 0.21$, $F(2, 29) =$

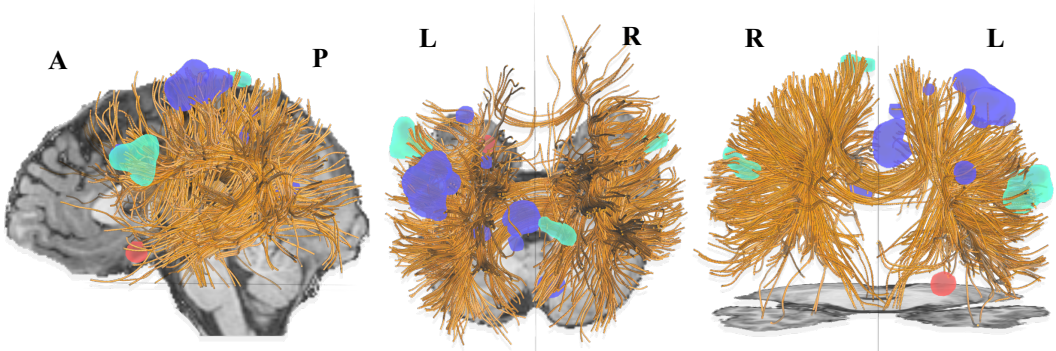

Figure 3: For visualization, fronto-parietal and parietal-temporal white matter are depicted with orange deterministic streamlines and significant dual-regression clusters ($p<0.05$ FWE) are shown in purple, green, and red. The anterior left amygdala, whose positive extrinsic connectivity with the fECN was positively associated with DR, is displayed in red. The right Precuneus, PCC, inferior Frontal Gyrus, and left somatosensory areas, whose negative intrinsic/extrinsic connectivity patterns were positively associated with DR, is displayed in purple. Lastly, the left Precentral Gyrus, left inferior Frontal Gyrus, and bilateral anterior Insula, whose negative intrinsic connectivity was positively associated with DR, are displayed in green.

2.62, $p<0.01$; $R^2 = 0.20$, $F(2, 29) = 2.36$, $p<0.01$)(*See* **Figure 3**). Additionally, average FA of the right SLFT and right SLFP, but not the bilateral CST or right CCG, was positively associated with total average connectivity of the pDMN ($R^2 = 0.36$, $F(2, 29) = 5.47$, $p<0.001$; $R^2 = 0.27$, $F(2, 29) = 3.48$, $p<0.01$). Finally, average FA of the right SLFT, and to a lesser extent the right SLFP, but not the bilateral CST or right CCG, negatively predicted the extrinsic connectivity of the fECN with the left Amygdala ($R^2 = 0.18$, $F(2, 29) = 2.07$, $p<0.05$; $R^2 = 0.13$, $F(2, 29) = 1.38$, $p<0.05$).

In sum, the global average FA measures of the right SLFP and especially the right SLFT predicted functional connectivity patterns of the triple-network associated with DR. When dual-regression was repeated using the tractography measures as predictors and constrained to the the three triple-network IC's only, we further found that average global FA of both the right SLFT and right SLFP predicted greater functional connectivity of each of the DR-associated triple-network clusters ($p<0.001$ uncorrected). We were also able to more precisely identify these multimodal relationships locally along each tract of interest by using the average total connectivity beta coefficients as regressors in voxel-wise TBSS. From that analysis, we found that FA within a small cluster at the Centrum Semiovale of the right anterior Corona Radiata (i.e. where crossing-fibers had earlier been found to be associated with DR), was also found to significantly predict total average connectivity of each of the triple-network RSN's ($p<0.05$, FWE)(*See light blue cluster* **Figure 4**). More precisely, we found that a posterior cluster of the right SLF was positively associated with functional connectivity of the fECN, whereas a medial cluster of the right SLF was

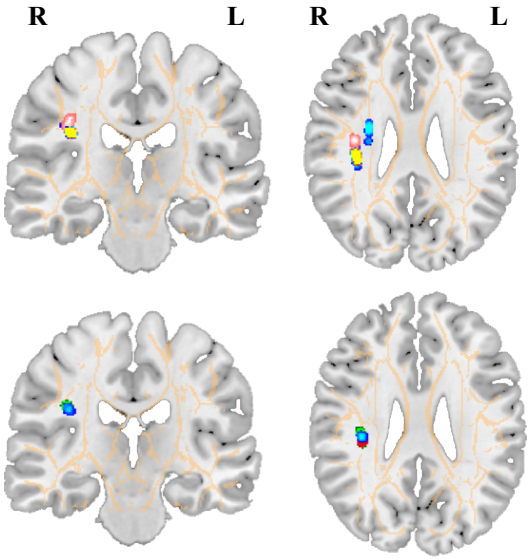

Figure 4: The above images depict correlations between RSN intrinsic/extrinsic functional connectivity and FA of the DR-associated right SLF fibers. The top row of images depicts a negative correlation between right medial SLFT FA and intrinsic connectivity of the coSN (pink) and pDMN (blue), as well as a positive correlation between FA and extrinsic connectivity of the right fECN (yellow) with the left Amygdala. The bottom row of images depicts the positive correlation between FA of crossing-fibers and these same intrinsic/extrinsic functional connectivity relationships.

negatively associated with functional connectivity of both the pDMN and coSN (*see* **Figure 4**). To confirm these relationships, we also found that the FA values of right medial SLFT crossing fibers were positively associated with the beta-weights of the DR-associated pDMN, coSN, and fECN clusters from dual-regression ($R^2 = 0.36$, $F(2, 32) = 8.97$, $p<0.001$; $R^2 = 0.31$, $F(2, 32) = 7.30$, $p<0.001$; $R^2 = 0.30$, $F(2, 32) = 6.71$, $p<0.001$).

Finally, we sought to determine whether microstructural connectivity of ROI's that emerged from our less conservative TBSS threshold (p=0.05 FWE) might also predict triple-network functional connectivity (*See* METHODS: **TBSS**). This exploratory analysis revealed that the DR-associated WM clusters of the CST, right CCG, right ATR, right UF, and Splenium each predicted functional connectivity of the DR-associated triple-network clusters from dual-regression as well (*See* Appendices, Results: **Section B**).

<u>'Between-Network' Functional Connectivity and Depressive Rumination</u>

FSLnets

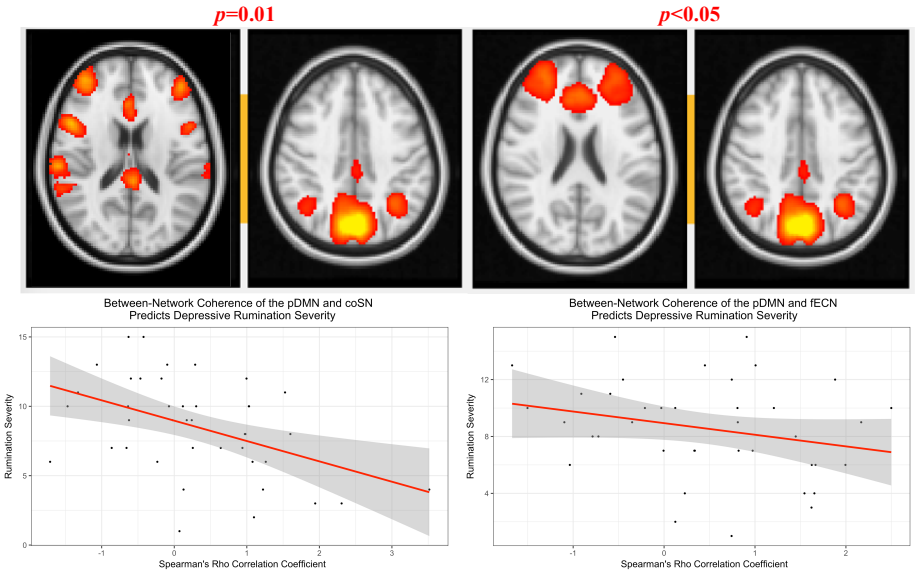

<u>Figure 5</u>: The top left two images depict an inverse correlation between the coSN and pDMN in association with DR. The right top two images depict a similar inverse correlation between the fECN and pDMN in association with DR. Finally, the bottom two plots depict each of these between-network inverse correlations positively associated with brooding scores.

Since several of the DR-associated functional connectivity clusters of the pDMN, coSN, and fECN were overlapping (e.g. at the left Precentral Gyrus), we next decided to explore whether the between-network functional connectivity correlation coefficients of each pair combination of triple-network RSN's was associated with DR. Although this could be done by

simply testing the interaction among all pairs of dual-regression clusters for each respective triple-network RSN, "recycling" the connectivity measures in this manner would introduce a bias since these measures were those already found to be associated with DR earlier in our analysis. Thus, we instead opted to report the between-network results from the glm_nets function in FSLnets, whereby partial correlations among all three RSN's effectively removed 'spurious' connectivity patterns within each raw triple-network IC to facilitate a FWE-corrected regression analysis for predicting higher brooding scores (*See* METHODS: **Between-Network Functional Connectivity**).

Randomise with FSLnets, restricted to only the triple-network RSN's, revealed that higher brooding scores were associated with greater inverse correlation between the fECN and pDMN ($p<0.05$, Bonferroni corrected), and between the coSN and the pDMN ($p<0.05$). The third 'between-network' correlation between fECN and coSN was not significantly associated with DR (*See* **Figure 5**).

WM Microstructure and 'Between-Network' Functional Connectivity

As with the functional connectivity findings, we also sought to test whether the WM microstructure findings informed by tractography and TBSS (both ROI-analysis and voxel-wise analysis) predicted the pDMN-fECN and pDMN-coSN inverse correlation coefficients from FSLnets.

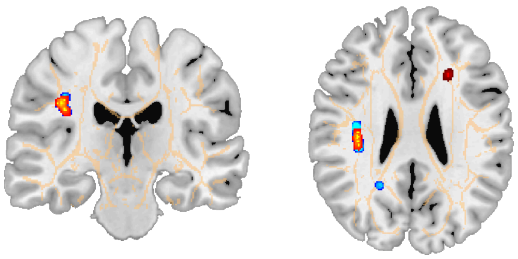

Figure 6: Lower FA of the right medial SLFT and the right posterior Corona Radiata (blue), as well as higher FA of right medial SLFT crossing fibers (red/yellow), was associated with greater pDMN-coSN inverse correlation. Similarly, lower FA of the left anterior Corona Radiata (red) was associated with greater pDMN-fECN inverse correlation.

Voxel-wise TBSS firstly revealed that the DR-associated pDMN-coSN inverse correlation predicted lower FA of a medial cluster of the right SLFT and another along the right posterior Corona Radiata ($p<0.01$ FWE)(*See red/yellow cluster* **Figure 6**). Correspondingly, lower FA of the left anterior Corona Radiata at a juncture where the left SLF meets the anterior Corpus Callosum predicted greater pDMN-fECN inverse correlation associated with DR. ($p<0.05$, FWE-corrected) (*See blue and red clusters* **Figure 6**).

We also found that FA values from the right crossing fibers of the anterior Corona Radiata (i.e. extracted from our earlier TBSS analysis) positively predicted the DR-associated

pDMN-coSN inverse correlation coefficients ($R^2 = 0.15$, $F(2, 32) = 2.92$, $p<0.05$). Likewise, our tractography measure of global average FA of the right SLFT also predicted the pDMN – coSN inverse correlation ($R^2 = 0.28$, $F(2, 29) = 3.39$, $p<0.01$).

As with the dual-regression findings, we sought to determine whether WM microstructure of ROI clusters that emerged from our less conservative TBSS threshold (p=0.05 FWE) might also predict the pDMN-coSN and pDMN-fECN inverse correlations associated with DR (*See* METHODS: **TBSS**). That analysis revealed that the DR-associated TBSS clusters of the bilateral CST, right CCG, right ATR, right UF, and Splenium each predicted the between-network inverse correlations coefficients of both the pDMN-coSN and pDMN-fECN (*See* Appendices, Results**: Section C**).

RESULTS: REPLICATION SAMPLE

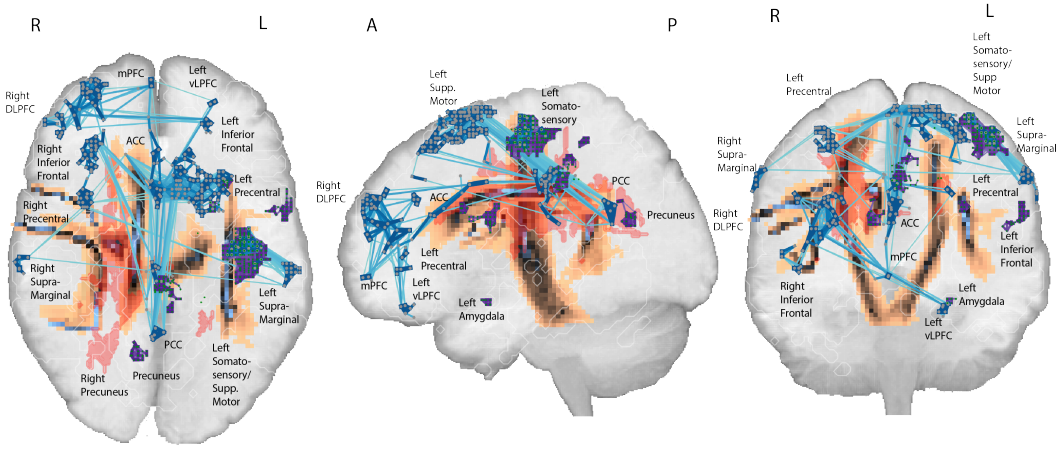

Figure 7: The above visualization summarizes key microstructural connectivity and functional connectivity biomarkers found to be associated with DR in the initial sample. Key fronto-parietal and parietal-temporal tracts revealed by tractography (right SLFT, right SLFP, left SLFT, right CCG, and bilateral CST) are represented in copper, with red contours depicting the strongest associations with DR along those tracts, as indicated from TBSS. The dual-regression clusters associated with DR are depicted in purple. Finally, 'triple network' connectivity of the pDMN, coSN, and fECN in combination are depicted here with blue lines and nodes.

Since RRS brooding scores in the NKI Rockland sample showed a significant positive skew, we performed a log transformation to yield a normal distribution. Following the application of a nearly identical analytic methdology to that used with our original sample (*See*

METHODS: **Replication**)**,** we were able to successfully replicate our findings across each level of analysis. Additionally, given the multiple scanner sites used to collect the neuroimaging data in the Rockland sample, we employed mixed-effects models (both with FSL's GLM and in R), whereby scanner site was modeled as a random effect.

Regression Findings (Predictor and Outcome)	Initial Sample	Replication Sample
Right SLFT Microstructure and DR Severity	TBSS (p<0.01 FWE, neg) Tractography (R^2=0.25, neg)	TBSS (p<0.01 FWE, neg) Tractography (R^2=0.30, neg)
Right SLFP Microstructure and DR Severity	TBSS (p<0.01 FWE, negative) Tractography (R^2=0.15, neg)	TBSS (p<0.01 FWE, neg) Tractography (R^2=0.19, neg)
Bilateral CST Microstructure and DR Severity	TBSS (p<0.01 FWE, negative) Tractography (R^2=0.12, neg)	TBSS (p<0.01 FWE, neg) Tractography (R^2=0.14, neg)
Right CCG Microstructure and DR Severity	TBSS (p<0.05 FWE, negative) Tractography (R^2=0.10, neg)	TBSS (p<0.01 FWE, neg) Tractography (R^2=0.22, neg)
Left UF Microstructure and DR Severity	TBSS (p<0.05 FWE, neg)	TBSS (p<0.01 FWE, neg) Tractography (R^2=0.23, neg)
Splenium of the Corpus Callosum Microstructure and DR Severity	TBSS (p<0.05 FWE, neg)	TBSS (p<0.05 FWE, neg)
Bilateral ATR Microstructure and DR Severity	TBSS (p<0.05 FWE, neg)	TBSS (p<0.05 FWE, neg)
Crossing-Fibers Microstructure and DR Severity	TBSS (p<0.05 FWE, CS of the SLF, pos)	TBSS (p<0.05 FWE, Corpus Callosum/left UF, pos)
pDMN Within-Network Connectivity and DR Severity	Dual-regression (p<0.01, FWE, neg)	Dual-regression (p<0.001, uncorrected, neg)
coSN Within-Network Connectivity and DR Severity	Dual-regression (p<0.01, FWE, neg)	Dual-regression (p<0.05, uncorrected, neg & pos)
fECN Within-Network Connectivity and DR Severity	Dual-regression (p<0.01, FWE, neg)	Dual-regression (p<0.001, uncorrected, neg)
pDMN-fECN Between-Network Connectivity and DR Severity	FSLnets (p<0.05, FWE, neg)	FSLnets (p<0.01, FWE, neg)
Right SLFT Microstructure and pDMN Within-Network Connectivity	Tractography (R^2=0.36, neg)	TBSS ROI-analysis (R^2=0.31, neg)
Right SLFT Microstructure and coSN Within-Network Connectivity	Tractography (R^2=0.21, neg)	TBSS ROI-analysis (R^2=0.20, neg)
Right SLFT Microstructure and fECN Within-Network Connectivity	Tractography (R^2=0.18, neg)	Tractography (R^2=0.26, pos) TBSS ROI-analysis (R^2=0.32, neg)
Right SLFP Microstructure and pDMN Within-Network Connectivity	Tractography (R^2=0.27, neg)	TBSS ROI-analysis (R^2=0.36, neg)
Right SLFP Microstructure and coSN Within-Network Connectivity	Tractography (R^2=0.20, neg)	Tractography (R^2=0.24, pos) TBSS ROI-analysis (R^2=-0.22, neg)
Right SLFP Microstructure and fECN Within-Network Connectivity	Tractography (R^2=0.13, neg)	Tractography (R^2=0.27, pos) TBSS ROI-analysis (R^2=0.31, pos)
CST Microstructure and pDMN Within-Network Connectivity	TBSS ROI-analysis (R^2=0.19, neg)	Tractography (R^2=0.19, neg) TBSS ROI-analysis (R^2=0.27, neg)
CST Microstructure and coSN Within-Network Connectivity	TBSS ROI-analysis (R^2=0.12, neg)	TBSS ROI-analysis (R^2=0.28, neg)
ATR Microstructure and pDMN Within-Network Connectivity	TBSS ROI-analysis (R^2=0.33, right, neg)	Tractography (R^2=0.23, neg) TBSS ROI-analysis (R^2=0.30, neg)
ATR Microstructure and coSN Within-Network Connectivity	TBSS ROI-analysis (R^2=0.21, right, neg)	Tractography (R^2=0.17, neg) TBSS ROI-analysis (R^2=0.23, neg)
Right CCG Microstructure and pDMN Within-Network Connectivity	TBSS ROI-analysis (R^2=0.29, neg)	Tractography (R^2=0.28, neg) TBSS ROI-analysis (R^2=0.29, neg)
Right CCG Microstructure and coSN Within-Network Connectivity	TBSS ROI-analysis (R^2=0.27, neg)	Tractography (R^2=0.15, neg)
Right CCG Microstructure and fECN Within-Network Connectivity	TBSS ROI-analysis (R^2=0.25, neg)	Tractography (R^2=0.23, pos) TBSS ROI-analysis (R^2=0.31, pos)
UF Microstructure and pDMN Within-Network Connectivity	TBSS ROI-analysis (R^2=0.29, right, neg)	Tractography (R^2=0.26, neg) TBSS ROI-analysis (R^2=0.22, neg)
UF Microstructure and fECN Within-Network Connectivity	TBSS ROI-analysis (R^2=0.22, right, neg)	TBSS ROI-analysis (R^2=0.15, left, pos)
UF Microstructure and fECN-coSN Between-Network Connectivity	Tractography (R2=0.23, right, neg) TBSS ROI-analysis (R^2=0.23, right, neg)	Tractography (R^2=0.37, left, pos)
Splenium Microstructure and pDMN Within-Network Connectivity	TBSS ROI-analysis (R^2=0.20, neg)	TBSS ROI-analysis (R^2=0.28, neg)
Secondary-Fiber Microstructure and pDMN Within-Network Connectivity	TBSS ROI-analysis (R^2=0.36, CS of the right SLF, pos)	TBSS ROI-analysis (R^2=0.32, Corpus Callosum, neg)

Table 1: The above table depicts each key finding (*left column*) that was significant in both the initial sample (*middle column*) and replication sample (*right column*). Each of the middle and right columns states the R^2 value from the respective regression models, the methodology used to estimate that value (e.g. TBSS ROI-analysis, tractography, dual-regression, FSLnets), and the directionality of the relationship (neg=negative, pos=positive). In total, 31 unique findings replicated either completely or partially across both samples.

dMRI Analyses (TBSS and Tractography)

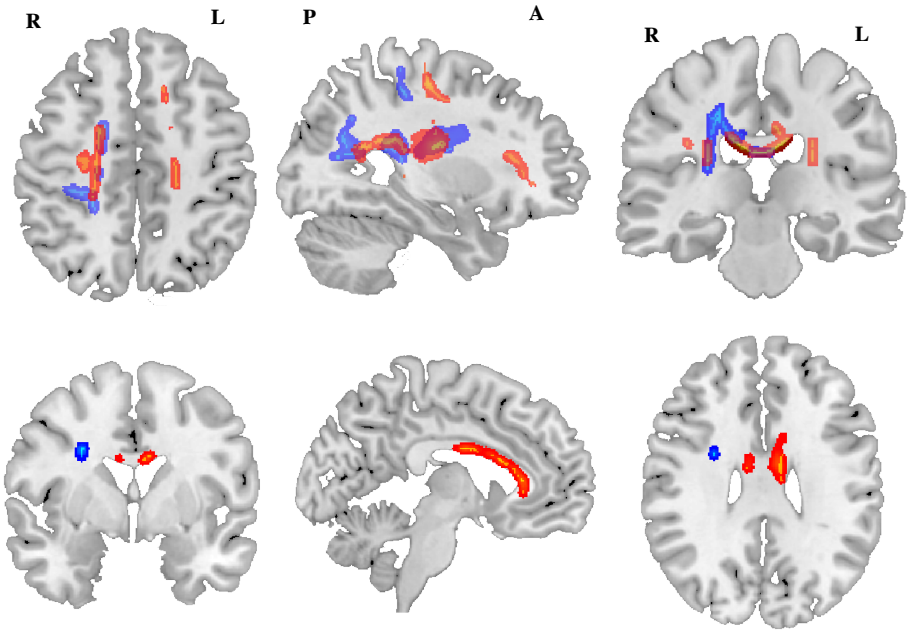

Figure 8 (colored, single column): Both rows of the above mosaic depict TBSS findings from the original sample (blue) and the NKI Rockland replication sample (red). The top row depicts the negative correlations in both samples between DR and FA (p=0.01 FWE in the initial sample, p=0.05 FWE in the replication sample). These findings overlapped very closely, albeit with greater coverage of the Corpus Callosum and left SLFT in the replication (red). The bottom row depicts the crossing-fibers findings in both samples which, unlike the FA findings, differed dramatically. Whereas DR was *positively* associated with secondary-fibers of the right anterior Corona Radiata at the Centrum Semiovale in the initial sample (blue), but *negatively* associated with secondary-fibers of Corpus Callosum, extending through the left anterior Corona Radiata in the replication sample (red)

The replication yielded a nearly equivalent set of dMRI findings using both TBSS and tractography methods, underscoring the high reproducibility of associations between WM microstructure and DR across samples. Using TBSS, we again found that FA of the right SLFT, SLFP, CCG, bilateral CST, and the body of the Corpus Callosum exhibited the strongest negative correlations with brooding scores (p<0.01, FWE) (*See* **Figure 8**). FA of the left UF and bilateral ATR also exhibited strong negative correlations with brooding scores (p<0.01, FWE), despite these WM clusters exhibiting weaker associations with DR in the initial sample. At the p=0.05 FWE threshold, 414 voxels were found to be overlapping in the TBSS results across samples. These voxels were primarily located in the right SLF, CST, and Corpus Callosum (*See top row* **Figure 8**). The subsequent 'crossing-fibers' TBSS analysis (*See* METHODS: **TBSS**; Appendices, Methods **B**), however, differed considerably across samples (*See* **Table 1 & 8**). In the initial sample, DR was *positively* associated with microstructure of secondary-fibers at the right anterior Corona Radiata; in the replication sample, it was *negatively* associated with

microstructure of secondary-fibers along the body of the Corpus Callosum and extending into the left anterior Corona Radiata (p<0.05 FWE)(*See* **Figure 8**). Despite these differences, the associations between secondary-fiber microstructure and DR across both samples were consistently within close anatomical proximity to the CST.

As in the initial sample, the tractography replication also demonstrated corresponding negative correlations between DR and average FA of the tracts of interest identified from TBSS. The correlation between DR and the right SLFT was again the strongest ($R^2 = 0.30$, p<0.01), whereas correlations with the bilateral CST ($R^2 = 0.14$, p<0.05), left UF ($R^2 = p$<0.05), right CCG ($R^2 = 0.22$, p<0.05) and right SLFP ($R^2 = 0.19$, $p < 0.05$) were weaker.

The initial within-network and between-network functional connectivity findings partially replicated using both dual-regression and FSLnets. Although similar functional connectivity patterns with DR were implied among the triple-network RSN's, the precise location of these clusters differed slightly across samples. The significant pDMN and coSN connectivity voxels associated with DR, for instance, were in close anatomical proximity across samples but not overlapping, whereas 9 voxels of the fECN positive connectivity cluster in the left amygdala/ parahippocampal gyrus cluster were overlapping. Lower pDMN functional connectivity of the right precuneus, bilateral insula/precentral gyri, and left parahippocampal gyrus clusters, but not the PCC cluster, replicated (p<0.01, uncorrected). Further, new clusters emerged in the replication sample that

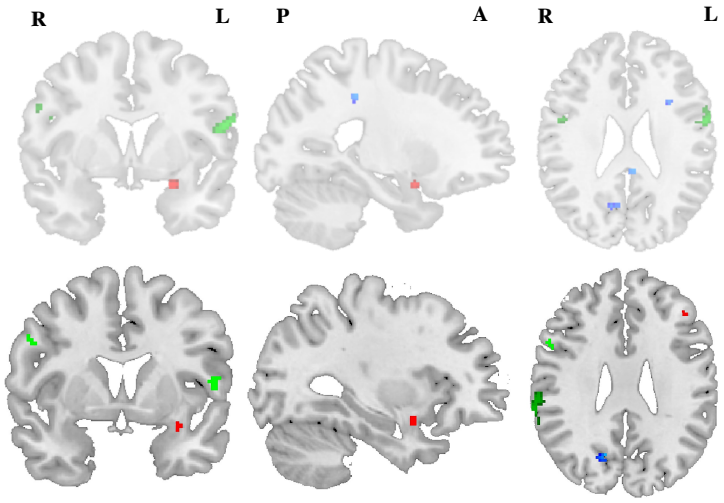

Figure 9 (colored, single column): Within-network connectivity findings from the Rockland NKI sample (bottom row) compared to those from the initial sample (top row). Significant clusters exhibiting lower functional connectivity within the pDMN associated with DR are depicted in blue. Significant right anterior Insula clusters exhibiting lower functional connectivity within the coSN are depicted in light green, and the right superior Temporal Gyrus cluster exhibiting higher functional connectivity within the coSN is depicted in dark green (right bottom row). Finally, significant clusters exhibiting greater functional connectivity within the fECN are depicted in red and include the left Amygdala/ parahippocampal Gyrus.

were not in the initial sample (e.g. a *positive* correlation between the coSN and an extrinsic cluster in the right superior temporal gyrus ($p<0.05$, uncorrected) as well as between the right DLPFC of the fECN and the left DLPFC ($p<0.01$, uncorrected) (*See* **Figure 9**). Unlike in the initial findings, however, within-network functional connectivity of the coSN was *both* positively and negatively associated with DR. With respect to between-network functional connectivity, the association between DR and the pDMN-fECN inverse correlation robustly replicated ($p<0.05$, FWE); the association between DR and the pDMN-coSN inverse correlation, on the other hand, did not. Additionally, we discovered a positive correlation between the fECN and the coSN ($p<0.05$, FWE) that was not observed in the initial sample. Hence, the pDMN-fECN inverse correlation associated with DR was consistent across samples, whereas the pDMN-coSN and fECN-coSN correlations associated with DR were *unique* to each sample.

Finally, when exploring multimodal microstructural-functional relationships in the replication sample, we found that average FA of numerous WM tracts again predicted both the between-network and within-network functional connectivity findings, but with some notable differences from the initial sample (*See* **Table 1** *and* Appendices, Results: **Section D** *for complete details*). Broadly speaking, we found that differences in secondary-fiber microstructure of the right anterior Corona Radiata appeared to explain these between-network functional connectivity differences across samples. Just as the secondary-fiber cluster of the SLF positively predicted the DR-associated pDMN-coSN inverse correlation in the initial sample (*See* **Figure 6**), a secondary-fiber cluster of the Corpus Callosum negatively predicted the DR-associated fECN-coSN correlation in the replication sample ($R^2 = 0.30$, $p<0.05$). Along these lines, microstructure of both secondary-fiber WM clusters strongly predicted the DR-associated within-network functional connectivity patterns of the pDMN across initial and replication samples ($R^2 = 0.36$, $p<0.001$**;** $R^2 = 0.46$, $p<0.001$).

Ultimately, WM microstructure predicted 24-26% of the variance in DR in both the initial and replication samples, with the majority of the contribution from the right SLF in both samples. The between-network functional connectivity patterns of the triple-network alone also collectively predicted nearly twice the variance (50-52%) in DR in both the initial and replication samples, when controlling for age and WM microstructure, and using the group-ICA RSN definitions from the initial sample.

DISCUSSION

The current study investigated associations between white matter (WM) microstructural connectivity, resting-state BOLD functional connectivity, and depressive rumination (DR) across two independent samples. The first sample consisted of thirty-nine adults with Major Depressive Disorder (MDD) and the second consisted of thirty-nine adults with MDD, equivalent measures of DR, demographic/inclusion criteria, and MRI data acquisition parameters (*See* METHODS: **Replication**). Findings from both samples converged on alterations in WM microstructure, aberrant functional connectivity patterns within and between the three resting-state networks of the 'triple-network', as well as interactions between microstructural connectivity and these functional connectivity patterns, all of which were associated with DR severity.

With respect to microstructural connectivity, DR severity was negatively associated with lower fractional anisotropy (FA) of the right Superior Longitudinal Fasciculus (SLF), right Cingulum (CCG), Corpus Callosum, and surrounding tracts like the Corticospinal Tract (CST), Splenium, Uncinate Fasciculus (UF), and Anterior Thalamic Radiation (ATR). Additionally, individual differences in DR severity were positively associated with FA of secondary 'crossing' fibers of the right anterior Corona Radiata (in the initial sample) and negatively associated with FA of crossing fibers of the Corpus Callosum extending into the left anterior Corona Radiata (in the replication sample). With respect to functional connectivity, DR severity was negatively associated with: 1) intrinsic functional connectivity of the posterior DMN (pDMN) and the Cingulo-Opercular SN (coSN), along with the inverse correlation between the pDMN and coSN networks as a whole (in the initial sample); 2) extrinsic connectivity of the fECN with the left Amygdala, along with the inverse correlation between the fECN and pDMN networks as a whole (in the replication sample).

With respect to the cross-modal relationship between microstructural and functional connectivity associated with DR severity, FA of primary-fibers for each of the DR-associated WM pathways predicted various aspects of intrinsic functional connectivity of the triple-network RSN's. In contrast, FA of secondary-fibers appeared to explain more complex individual differences in between-network functional connectivity of the triple-network associated with DR severity across samples.

WM Microstructure and Depressive Rumination

A growing body of literature on the role of the SLF in disordered behavior may help to explain our core dMRI finding that DR was associated with microstructural connectivity of the SLF. Previous research has shown, for instance, that the SLF is associated with longer and more severe depressive episodes in MDD[76]. Deeper insights might also be gleaned, however, from the fine-grained dMRI analyses employed in the present study. Tractography revealed, for instance, that DR was associated with two sub-divisions of the SLF itself: 1) an inferior portion connecting the middle/superior Temporal Gyrus with ipsilateral prefrontal/cingulo-opercular areas referred to as the SLFT, which most closely corresponds to SLF III/Arcuate Fasciculus; and 2) a superior portion connecting the Supramarginal Gyrus of the Parietal Lobe to dorsal, ipsilateral prefrontal regions, referred to as the SLFP, which most closely corresponds to the SLF II[77]. In connecting the PFC with the Parietal Lobe, the SLFP may support interactions between the DLPFC and Parietal Lobe in order to regulate spatial attention[78]. In the context of DR, diminished microstructural connectivity of the SLFP could reflect disrupted internal-external attention shifting, whereby self-referential processing dominates attention[79]. In contrast, the SLFT is involved in the communication of semantic content between the parietal and frontal lobes, and is thought to maintain phonological awareness[78,80]. As confirmed through tests of hemisphericity, microstructural connectivity deficits of the *right* SLFT in particular were most strongly associated with DR. Accordingly, studies have suggested that the right SLF may provide compensatory support for increased demands on language and higher-cognitive thought[81,82], though more research on the role of the right temporal SLF in particular is still needed. Still, cortical areas connected by the right SLFT such as the right Temporoparietal Junction and right superior Temporal Gyrus have been implicated in monological speech faculties[83], which is also generally assumed to be integral to the self-referential processing disrupted in DR[9,84].

The only prior TBSS analysis of DR[32] also found that diminished SLF microstructural connectivity was associated with DR severity, but in the *left* hemisphere. Nevertheless, culture-specific individual differences between our English-speaking participants and that study's Mandarin-speaking participants might explain this discrepancy. Specifically, self-referential processing of Mandarin speakers may operate contra-laterally to that of English speakers, since

more tonal Chinese characters recruit greater right superior Temporal Gyrus activity, whereas more atonal English words do not[35].

Finally, TBSS also revealed a strong association between DR severity and microstructural connectivity of secondary-fibers. In the initial sample, for instance, there was a positive association between secondary-fibers of the anterior Corona Radiata and Corpus Callosum. These pathways are sensitive to bodily sensations transmitted via the CST, but also to salience signaling by neighboring cingulo-opercular structures, particularly the ACC[85,86]. Given that vast individual differences are believed to exist in the microstructure of WM crossing-fibers[62], moreover, our findings indicate that secondary-fibers might assume a variety of pathological configurations that confer a risk for DR.

Within-Network Functional Connectivity and Depressive Rumination

The results from our functional connectivity analyses broadly implied that an imbalance of functional integration and segregation of self-referential, salience, and cognitive control systems are associated with DR. These relationships were observed both by way of lower intrinsic and extrinsic connectivity of the pDMN, coSN, and fECN, respectively.

<u>pDMN</u>

The association between higher DR severity and lower functional connectivity within the pDMN was characterized by two key features: 1) lower intrinsic connectivity of the right Precuneus with other nodes of the pDMN; 2) lower extrinsic connectivity of the pDMN with the left Somatosensory Cortex, left inferior Frontal Gyrus, and left Precentral Gyrus. Given the extent of these functional connectivity disturbances of the pDMN, most of which directly and completely replicated (*See* **Table 1**), our findings imply globally segregated and dysregulated self-referential processing associated with DR, which is highly consistent with prior work[36,87].

<u>fECN</u>

Higher DR severity was also associated with greater extrinsic functional connectivity between the fECN and the left Amygdala/ Parahippocampal gyrus – a finding that replicated closely across samples, and would appear to support the theory of impaired disengagement as at least a partial explanation of DR[88]. Aligned with this interpretation, our findings robustly support the notion that the negatively-biased self-referential processing of DR may become perseverative and prolonged through impaired top-down cognitive control of subcortical limbic structures[89]. Additionally, our cross-modal findings showed that decreased microstructural

connectivity between the ACC and right DLPFC (via right dorsal UF, ATR, and anterior CCG) was associated with the DR-associated increase in fECN-limbic functional connectivity, suggesting that weaker structural connections within this cognitive control circuit confer a higher risk for impaired disengagement in DR as well.

coSN

Lower functional connectivity with the right anterior Insula was found to be associated with higher DR severity across both samples and likely represents a robust coSN biomarker of DR. On the one hand, lower coSN functional connectivity of the right anterior Insula may indicate difficulty sustaining vigilant attentional states[90] in DR (i.e. regardless of positive or negative salience). By that interpretation, competing internal responses received from ventral autonomic structures might serve to interrupt tonic alertness in DR[91]. Indeed, our findings also showed that microstructural connectivity of ATR fibers linking the ACC to the basal ganglia circuit positively predicted lower coSN functional connectivity and was negatively associated with DR severity. On the other hand, lower coSN functional connectivity of the right anterior Insula might more broadly reflect disrupted coordination of the DMN and ECN in DR, particularly since the right anterior Insula is known to be responsible for synchronizing toggling between task-negative and task-positive networks[37,43].

Between-Network Functional Connectivity and Depressive Rumination

Upon discovering spatially-overlapping patterns of aberrant extrinsic functional connectivity among the triple-network RSN's, we then found that DR severity was additionally associated with patterns of *between*-network functional connectivity, whose variance was further explained by patterns of WM microstructural connectivity as well. Specifically, higher DR severity was associated with greater inverse correlation between the pDMN-fECN in both initial and replication samples, greater inverse correlation between the pDMN-coSN in the initial sample, and greater direct correlation between the fECN-coSN in the replication sample. As our cross-modal analyses suggested, moreover, the pDMN-coSN and fECN-coSN between-network correlation patterns were largely susceptible to individual differences in secondary-fiber microstructural connectivity, whereas the pDMN-fECN inverse correlation was not.

pDMN-fECN

The pDMN-fECN finding partially replicates prior work showing that greater functional dominance of the DMN over the ECN is associated with higher DR[45,92]. Since the pDMN is

functionally coupled with the hippocampus during memory retrieval[38] and the Parahippocampal Gyrus was found to be less functionally connected to the fECN, greater pDMN-fECN inverse correlation associated with higher DR severity could reflect a failure to regulate the episodic memory refreshing that is thought to occur during self-referential processing[93].

Not only did these pDMN-fECN findings replicate prior work[43,45], but they also replicated across both our initial and replication samples, which underscores a consistent pattern of antagonism between self-referential and cognitive control systems as a defining feature of DR. As with the multimodal relationships discovered when exploring each triple-network RSN separately, tractography also revealed that microstructural connectivity of the right SLFT predicted the pDMN-fECN inverse correlation in both samples. Likewise, TBSS showed that the pDMN-fECN inverse correlation was associated with lower microstructural connectivity of the left anterior Corona Radiata, which supplies connections between the ACC and the DLPFC, and may be relevant for cognitive control of emotion and working memory[91,94].

<u>fECN-coSN and pDMN-coSN</u>

The SN is important for switching attention between externally and internally salient stimuli[37,95] and our findings indicated that disruptions with respect to its relationship with each of the pDMN and fECN confers a risk for DR. Along these lines, exploratory TBSS analyses revealed that the fECN-coSN and pDMN-coSN between-network functional connectivity patterns may be a by-product of microstructural connectivity deficits of the right medial SLFT, but may more precisely reflect individual differences in microstructural connectivity of bilateral anterior Corona Radiata secondary fibers where the SLFT intersects with the Corpus Callosum in proximity to the ACC (*See* **Figure 6**). Specifically, the initial sample showed greater microstructural connectivity of right anterior Corona Radiata secondary fibers, whereas the replication sample showed lower microstructural connectivity of the Corpus Callosum and left anterior Corona Radiata (*See* **Figure 8**). In support of those findings, prior work has shown that secondary-fiber microstructure of the SLF and SN-DMN interactions may be related[43,96]; likewise, disrupted corpus callosal WM and SN-ECN interactions may also be related[97,98]. Since the anterior Corona Radiata is believe to connect language and interhemispheric communication pathways[99], associated aberrant triple-network functional connectivity patterns might indicate that corresponding salience, self-referential, cognitive control mechanisms of DR are subject to individual differences in the capacity to utilize both brain hemispheres to support language

processing. This variability of DR-associated secondary-fibers across initial and replication samples, and the associated relative dominance of pDMN-coSN versus fECN-coSN disturbances, respectively, could therefore suggest that individual differences in secondary-fiber microstructure may confer variable risk for DR over and above the other DR biomarkers discussed. Future studies should utilize larger sample sizes to explore these complex between-network relationships further and more thoroughly examine associated secondary-fiber subtypes of in the brains of depressed ruminators.

CONCLUSION

This study aimed to identify microstructural and functional network connectivity biomarkers of depressive rumination (DR) in MDD that could be demonstrated across two independent samples. Our findings from both datasets demonstrated that higher DR severity is associated with lower White-Matter (WM) microstructural connectivity of the right SLF, along with several surrounding primary and secondary-fiber clusters. Our findings also showed that higher DR severity is associated with aberrant functional connectivity of the 'triple-network', here defined as consisting of the precuneal Default Mode Network (pDMN), cingulo-opercular Salience Network (coSN), and frontal Executive Control Network (fECN). These functional connectivity disturbances included: 1) lower intrinsic functional connectivity of the pDMN and the coSN, along with higher inverse correlation between the pDMN and coSN networks as a whole; 2) higher extrinsic connectivity of the fECN with the left Amygdala/ Parahippocampal Gyrus; 3) greater inverse correlation between fECN and pDMN networks, but also aberrant correlations between the coSN and each of the pDMN and fECN, depending on underlying secondary-fiber microstructure of the anterior Corona Radiata. Taken together, these findings appear to indicate that microstructural connections broadly supporting inward attention, affective sensitivity, and language processing efficiency, constrain maladaptive functional interactions among self-referential, salience, and cognitive control systems at fault in DR. Ultimately, our analyses suggest that a complex neurobiological interplay between microstructural connectivity and functional connectivity of the triple-network confers a multivariate risk for DR.

Supported by initial discovery plus replication, our findings enhance existing research on the neurobiological substrates of trait rumination in MDD. Perhaps most notably, we demonstrate that neural pathophysiological models of DR that accommodate for individual

differences cannot be reduced to singular, unimodal mechanisms. Rather, a unified[9], precise[100], and reproducible[54] neurobiology of DR need be construed as the confluence of multimodal mechanisms, implicating both microstructural and functional network connectivity, and corresponding to multiple distinct, yet interactive, cognitive mechanisms.

ACKNOWLEDGMENTS

The authors would first like to thank the technical staff at the Texas Advanced Computing Center (TACC) for supplying the computational resources and consulting that would have otherwise rendered our neuroimaging analyses computationally intractable. We would also like to thank Ryan Hammonds for assistance with quality control of neuroimaging data. Additionally, the first author would also like to thank Ari Cohen for her incredible patience and support throughout drafting of the manuscript.

FUNDING

This work was supported by the R21 MH092430 award to Christopher G. Beevers.

COMPETING INTERESTS

We wish to confirm that there are no known conflicts of interest associated with this manuscript and there has been no significant financial support for this work that could have influenced its outcome.

MATERIALS AND CORRESPONDENCE

All materials and correspondence should be addressed to the first author, Derek Pisner, at dpisner@utexas.edu

REFERENCES

1. Beevers, C. G. Cognitive vulnerability to depression: A dual process model. *Clinical Psychology Review* **25,** 975–1002 (2005).
2. Nolen-Hoeksema, S. & Morrow, J. A prospective study of depression and posttraumatic stress symptoms after a natural disaster: the 1989 Loma Prieta Earthquake. *J. Pers. Soc. Psychol.* **61,** 115–121 (1991).
3. Nolen-hoeksema, S. Further Evidence for the Role of Psychosocial additional foci for future research . *Clin. Psychol. Sci. Pract.* **7,** 224–227 (2000).
4. Nolen-Hoeksema, S., Wisco, B. E. & Lyubomirsky, S. Rethinking Rumination. *Perspect.*

Psychol. Sci. **3,** 400–424 (2008).
5. Watkins, E. Psychological treatment of depressive rumination. *Current Opinion in Psychology* **4,** 32–36 (2015).
6. Wells, A. & Papageorgiou, C. in *Depressive Rumination: Nature, Theory and Treatment* 259–273 (2008).
7. Woody, M. L. & Gibb, B. E. Integrating NIMH Research Domain Criteria (RDoC) into depression research. *Current Opinion in Psychology* **4,** 6–12 (2015).
8. Schnyer, D. M. *et al.* Neurocognitive therapeutics: from concept to application in the treatment of negative attention bias. *Biol. mood {&} anxiety Disord.* **5,** 1 (2015).
9. Nejad, A. B., Fossati, P. & Lemogne, C. Self-referential processing, rumination, and cortical midline structures in major depression. *Front. Hum. Neurosci.* **7,** 666 (2013).
10. Brewer, J. A., Garrison, K. A. & Whitfield-Gabrieli, S. What about the 'Self' is Processed in the Posterior Cingulate Cortex? *Front. Hum. Neurosci.* **7,** (2013).
11. Yoshimura, S. *et al.* Self-referential processing of negative stimuli within the ventral anterior cingulate gyrus and right amygdala. *Brain Cogn.* **69,** 218–225 (2009).
12. Watkins, E. & Teasdale, J. D. Rumination and overgeneral memory in depression: Effects of self-focus and analytic thinking. *J. Abnorm. Psychol.* **110,** 353–357 (2001).
13. Machino, A. *et al.* Possible involvement of rumination in gray matter abnormalities in persistent symptoms of major depression: an exploratory magnetic resonance imaging voxel-based morphometry study. *J. Affect. Disord.* **168,** 229–235 (2014).
14. Jung-Beeman, M. *et al.* Neural activity when people solve verbal problems with insight. *PLoS Biol.* **2,** (2004).
15. Siegle, G. J., Steinhauer, S. R., Thase, M. E., Stenger, V. A. & Carter, C. S. Can't shake that feeling… *Biol. Psychiatry* **51,** 693–707 (2002).
16. Mandell, D., Siegle, G. J., Shutt, L., Feldmiller, J. & Thase, M. E. Neural substrates of trait ruminations in depression. *J. Abnorm. Psychol.* **123,** 35–48 (2014).
17. Kühn, S., Vanderhasselt, M. A., De Raedt, R. & Gallinat, J. Why ruminators won't stop: The structural and resting state correlates of rumination and its relation to depression. *J. Affect. Disord.* **141,** 352–360 (2012).
18. Cooney, R. E., Joormann, J., Eugène, F., Dennis, E. L. & Gotlib, I. H. Neural correlates of rumination in depression. *Cogn. Affect. Behav. Neurosci.* **10,** 470–8 (2010).
19. Kolling, N., Behrens, T. E. J., Wittmann, M. K. & Rushworth, M. F. S. Multiple signals in anterior cingulate cortex. *Curr. Opin. Neurobiol.* **37,** 36–43 (2016).
20. Stevens, F. L., Hurley, R. A. & Taber, K. H. Anterior Cingulate Cortex: Unique Role in Cognition and Emotion. *J. Neuropsychiatry Clin. Neurosci.* **23,** 121–125 (2011).
21. Etkin, a, Egner, T. & Kalisch, R. Emotional processing in anterior cingulate and medial prefrontal. *Trends Cogn. Sci.* **15,** 85–93 (2011).
22. Southworth, F., Grafton, B., MacLeod, C. & Watkins, E. Heightened ruminative disposition is associated with impaired attentional disengagement from negative relative to positive information: support for the 'impaired disengagement' hypothesis. *Cogn. Emot.* **31,** 422–434 (2017).
23. Koster, E. H. W., De Lissnyder, E., Derakshan, N. & De Raedt, R. Understanding depressive rumination from a cognitive science perspective: The impaired disengagement hypothesis. *Clinical Psychology Review* **31,** 138–145 (2011).
24. Bernstein, E. E., Heeren, A. & McNally, R. J. Unpacking Rumination and Executive Control: A Network Perspective. *Clin. Psychol. Sci.* 216770261770271 (2017).

25. Rude, S. S., Maestas, K. L. & Neff, K. Paying attention to distress: What's wrong with rumination? *Cogn. Emot.* **21,** 843–864 (2007).
26. Wang, K. *et al.* Individual differences in rumination in healthy and depressive samples: Association with brain structure, functional connectivity and depression. *Psychol. Med.* **45,** 2999–3008 (2015).
27. Jacobs, R. H. *et al.* Targeting ruminative thinking in adolescents at risk for depressive relapse: Rumination-focused cognitive behavior therapy in a pilot randomized controlled trial with resting state fMRI. *PLoS One* **11,** (2016).
28. Monnart, A., Kornreich, C., Verbanck, P. & Campanella, S. Just swap out of negative vibes? Rumination and inhibition deficits in major depressive disorder: Data from event-related potentials studies. *Frontiers in Psychology* **7,** (2016).
29. Stephan, K. E. *et al.* Lateralized cognitive processes and lateralized task control in the human brain. *Science (80-.).* **301,** 384–386 (2003).
30. Ordaz, S. J. *et al.* Ruminative brooding is associated with salience network coherence in early pubertal youth. *Soc. Cogn. Affect. Neurosci.* nsw133 (2016).
31. Hamilton, J. P., Farmer, M., Fogelman, P. & Gotlib, I. H. Depressive Rumination, the Default-Mode Network, and the Dark Matter of Clinical Neuroscience. *Biological Psychiatry* **78,** 224–230 (2015).
32. Zuo, N. *et al.* White matter abnormalities in major depression: A tract-based spatial statistics and rumination study. *PLoS One* **7,** (2012).
33. Yendiki, A. *et al.* Automated probabilistic reconstruction of white-matter pathways in health and disease using an atlas of the underlying anatomy. *Front. Neuroinform.* **5,** 23 (2011).
34. Pennebaker, J. W. & King, L. a. Linguistic styles: Language use as an individual difference. *J. Pers. Soc. Psychol.* **77,** 1296–1312 (1999).
35. Crinion, J. T. *et al.* Neuroanatomical markers of speaking Chinese. *Hum. Brain Mapp.* **30,** 4108–4115 (2009).
36. Rosenbaum, D. *et al.* Aberrant functional connectivity in depression as an index of state and trait rumination. *Sci. Rep.* **7,** 2174 (2017).
37. Menon, V. Large-scale brain networks and psychopathology: A unifying triple network model. *Trends in Cognitive Sciences* **15,** 483–506 (2011).
38. Huijbers, W., Pennartz, C. M. A., Cabeza, R. & Daselaar, S. M. The hippocampus is coupled with the default network during memory retrieval but not during memory encoding. *PLoS One* **6,** (2011).
39. Sheline, Y. I. *et al.* The default mode network and self-referential processes in depression. *Proc. Natl. Acad. Sci. U. S. A.* **106,** 1942–1947 (2009).
40. Yang, Y. *et al.* Task and resting-state fMRI reveal altered salience responses to positive stimuli in patients with major depressive disorder. *PLoS One* **11,** 1–19 (2016).
41. Kocsel, N. *et al.* Trait Rumination Influences Neural Correlates of the Anticipation but Not the Consumption Phase of Reward Processing. *Front. Behav. Neurosci.* **11,** (2017).
42. Menon, V. & Uddin, L. Q. Saliency, switching, attention and control: a network model of insula function. *Brain Struct. Funct.* **214,** 655–667 (2010).
43. Liang, X. *et al.* Interactions between the Salience and Default-Mode Networks Are Disrupted in Cocaine Addiction. *J. Neurosci.* **35,** 8081–8090 (2015).
44. Cohen, N. *et al.* Using executive control training to suppress amygdala reactivity to aversive information. *Neuroimage* **125,** 1022–1031 (2016).

45. Hamilton, J. P. *et al*. Default-mode and task-positive network activity in major depressive disorder: Implications for adaptive and maladaptive rumination. *Biol. Psychiatry* **70,** 327–333 (2011).
46. Burkhouse, K. L. *et al*. Neural correlates of rumination in adolescents with remitted major depressive disorder and healthy controls. *Cogn. Affect. Behav. Neurosci.* **17,** 394–405 (2017).
47. Tao, Y. *et al*. The Structural Connectivity Pattern of the Default Mode Network and Its Association with Memory and Anxiety. *Front. Neuroanat.* **9,** (2015).
48. Steffens, D. C., Taylor, W. D., Denny, K. L., Bergman, S. R. & Wang, L. Structural integrity of the uncinate fasciculus and resting state functional connectivity of the ventral prefrontal cortex in late life depression. *PLoS One* **6,** (2011).
49. Braun, U. *et al*. From Maps to Multi-dimensional Network Mechanisms of Mental Disorders. *Neuron* **97,** 14–31 (2018).
50. Bassett, D. S. & Gazzaniga, M. S. Understanding complexity in the human brain. *Trends in Cognitive Sciences* **15,** 200–209 (2011).
51. Button, K. S. *et al*. Power failure: Why small sample size undermines the reliability of neuroscience. *Nat. Rev. Neurosci.* **14,** 365–376 (2013).
52. Mulugeta, L. *et al*. Credibility, Replicability, and Reproducibility in Simulation for Biomedicine and Clinical Applications in Neuroscience. **12,** 1–16 (2018).
53. Nooner, K. B. *et al*. The NKI-Rockland sample: A model for accelerating the pace of discovery science in psychiatry. *Frontiers in Neuroscience* (2012).
54. Poldrack, R. A. *et al*. Scanning the horizon: Towards transparent and reproducible neuroimaging research. *Nat. Rev. Neurosci.* **18,** 115–126 (2017).
55. Sheehan, D. V. *et al*. The Mini-International Neuropsychiatric Interview (M.I.N.I.): The development and validation of a structured diagnostic psychiatric interview for DSM-IV and ICD-10. in *Journal of Clinical Psychiatry* **59,** 22–33 (1998).
56. First, M. B., Gibbon, M., Spitzer, R. L., Gibbon, M. & Williams, J. B. W. in *American Psychiatric Press, Inc.* (1997).
57. Beevers, C. G., Clasen, P. C., Enock, P. M. & Schnyer, D. M. Attention bias modification for major depressive disorder: Effects on attention bias, resting state connectivity, and symptom change. *J. Abnorm. Psychol.* **124,** 463–475 (2015).
58. Erdur-Bakera, Ö.¨ & Bugaya, A. The short version of ruminative response scale: Reliability, validity and its relation to psychological symptoms. in *Procedia - Social and Behavioral Sciences* **5,** 2178–2181 (2010).
59. Treynor, W., Gonzalez, R. & Nolen-Hoeksema, S. Rumination reconsidered: A psychometric analysis. *Cognit. Ther. Res.* **27,** 247–259 (2003).
60. Jenkinson, M., Beckmann, C. F., Behrens, T. E. J., Woolrich, M. W. & Smith, S. M. FSL. *NeuroImage* **62,** 782–790 (2012).
61. Smith, S. M. *et al*. Tract-based spatial statistics: Voxelwise analysis of multi-subject diffusion data. *Neuroimage* **31,** 1487–1505 (2006).
62. Jbabdi, S., Behrens, T. E. J. & Smith, S. M. Crossing fibres in tract-based spatial statistics. *Neuroimage* **49,** 249–256 (2010).
63. Westlye, L. T. *et al*. Life-span changes of the human brain white matter: diffusion tensor imaging (DTI) and volumetry. *Cereb. Cortex* **20,** 2055–2068 (2010).
64. Nolen-Hoeksema, S. Sex Differences in Unipolar Depression: Evidence and Theory. *Psychological Bulletin* **101,** 259–282 (1987).

65. De Groot, M. *et al*. Improving alignment in Tract-based spatial statistics: Evaluation and optimization of image registration. *Neuroimage* **76,** 400–411 (2013).
66. Torgerson, C. M. *et al*. DTI tractography and white matter fiber tract characteristics in euthymic bipolar I patients and healthy control subjects. *Brain Imaging Behav*. **7,** 129–139 (2013).
67. Vernooij, M. W. *et al*. Fiber density asymmetry of the arcuate fasciculus in relation to functional hemispheric language lateralization in both right- and left-handed healthy subjects: A combined fMRI and DTI study. *Neuroimage* **35,** 1064–1076 (2007).
68. Beckmann, Mackay, Filippini & Smith. Group comparison of resting-state FMRI data using multi-subject ICA and dual regression. *Neuroimage* **47,** S148 (2009).
69. Thomas Yeo, B. T. *et al*. The organization of the human cerebral cortex estimated by intrinsic functional connectivity. *J. Neurophysiol*. **106,** 1125–1165 (2011).
70. Wu, X. *et al*. A triple network connectivity study of large-scale brain systems in cognitively normal APOE4 carriers. *Front. Aging Neurosci*. **8,** (2016).
71. Watkins, E. & Brown, R. G. Rumination and executive function in depression: an experimental study. *J. Neurol. Neurosurg. Psychiatry* **72,** 400–2 (2002).
72. Dutta, A., McKie, S. & Deakin, J. F. W. Resting state networks in major depressive disorder. *Psychiatry Res*. **224,** 139–51 (2014).
73. Smith, S. M. The future of FMRI connectivity. *NeuroImage* **62,** 1257–1266 (2012).
74. Smith, S. M. & Nichols, T. E. Threshold-free cluster enhancement: Addressing problems of smoothing, threshold dependence and localisation in cluster inference. *Neuroimage* **44,** 83–98 (2009).
75. Smith, S. FSLnets. *FMRIB Software Library v5.0* Available at: https://fsl.fmrib.ox.ac.uk/fsl/fslwiki/FSLNets.
76. Lai, C. H. & Wu, Y. T. Alterations in white matter micro-integrity of the superior longitudinal fasciculus and anterior thalamic radiation of young adult patients with depression. *Psychol. Med*. **44,** 2825–2832 (2014).
77. Wakana, S. *et al*. Reproducibility of quantitative tractography methods applied to cerebral white matter. *Neuroimage* **36,** 630–644 (2007).
78. Jenkins, L. M. *et al*. Shared white matter alterations across emotional disorders: A voxel-based meta-analysis of fractional anisotropy. *NeuroImage Clin*. **12,** 1022–1034 (2016).
79. Wagner, G. *et al*. Self-referential processing influences functional activation during cognitive control: An fMRI study. *Soc. Cogn. Affect. Neurosci*. **8,** 828–837 (2013).
80. Oechslin, M. S., Imfeld, A., Loenneker, T., Meyer, M. & Jäncke, L. The plasticity of the superior longitudinal fasciculus as a function of musical expertise: a diffusion tensor imaging study. *Front. Hum. Neurosci*. **3,** 76 (2009).
81. Glasser, M. F. & Rilling, J. K. DTI tractography of the human brain's language pathways. *Cereb. Cortex* **18,** 2471–2482 (2008).
82. Lindell, A. K. In your right mind: Right hemisphere contributions to language processing and production. *Neuropsychol. Rev*. **16,** 131–148 (2006).
83. Geva, S. *et al*. The neural correlates of inner speech defined by voxel-based lesion-symptom mapping. *Brain* **134,** 3071–3082 (2011).
84. Alderson-Day, B. & Fernyhough, C. Inner speech: Development, cognitive functions, phenomenology, and neurobiology. *Psychol. Bull*. **141,** 931–965 (2015).
85. Huang, L. a *et al*. Study of white matter at the centrum semiovale level with magnetic resonance spectroscopy and diffusion tensor imaging in cerebral small vessel disease.

Genet. Mol. Res. **13,** 2683–90 (2014).
86. Sacchet, M. D. *et al.* Structural abnormality of the corticospinal tract in major depressive disorder. *Biol. Mood Anxiety Disord.* **4,** 8 (2014).
87. Klaassens, B. L. *et al.* Diminished Posterior Precuneus Connectivity with the Default Mode Network Differentiates Normal Aging from Alzheimer's Disease. *Front. Aging Neurosci.* **9,** 97 (2017).
88. Koster, E. H. W., De Raedt, R., Goeleven, E., Franck, E. & Crombez, G. Mood-congruent attentional bias in dysphoria: maintained attention to and impaired disengagement from negative information. *Emotion* **5,** 446–455 (2005).
89. Daniels, J. K. *et al.* Switching between executive and default mode networks in posttraumatic stress disorder: Alterations in functional connectivity. *J. Psychiatry Neurosci.* **35,** 258–266 (2010).
90. Sadaghiani, S. & D'Esposito, M. Functional characterization of the cingulo-opercular network in the maintenance of tonic alertness. *Cereb. Cortex* **25,** 2763–2773 (2015).
91. Cohen, J. D., Botvinick, M. & Carter, C. S. Anterior cingulate and prefrontal cortex: who's in control? *Nat. Neurosci.* **3,** 421–423 (2000).
92. Wang, X., Öngür, D., Auerbach, R. P. & Yao, S. Cognitive Vulnerability to Major Depression: View from the Intrinsic Network and Cross-network Interactions. *Harv. Rev. Psychiatry* **24,** 188–201 (2016).
93. Züst, M. A. *et al.* Hippocampus is place of interaction between unconscious and conscious memories. *PLoS One* **10,** (2015).
94. Niogi, S. N. *et al.* Structural dissociation of attentional control and memory in adults with and without mild traumatic brain injury. *Brain* **131,** 3209–3221 (2008).
95. Uddin, L. Q. Salience Network Dysfunction. *Salience Netw. Hum. Brain* 23–28 (2017).
96. Morie, K. P. *et al.* White-matter crossing-fiber microstructure in adolescents prenatally exposed to cocaine. *Drug Alcohol Depend.* **174,** 23–29 (2017).
97. Bonnelle, V. *et al.* Salience network integrity predicts default mode network function after traumatic brain injury. *Proc. Natl. Acad. Sci.* **109,** 4690–4695 (2012).
98. Yuan, K. *et al.* Reduced Fractional Anisotropy of Corpus Callosum Modulates Inter-Hemispheric Resting State Functional Connectivity in Migraine Patients without Aura. *PLoS One* **7,** (2012).
99. Sanjuan, P. M., Thoma, R., Claus, E. D., Mays, N. & Caprihan, A. Reduced white matter integrity in the cingulum and anterior corona radiata in posttraumatic stress disorder in male combat veterans: A diffusion tensor imaging study. *Psychiatry Res. - Neuroimaging* **214,** 260–268 (2013).
100. Friston, K. J. Precision Psychiatry. *Biological Psychiatry: Cognitive Neuroscience and Neuroimaging* **2,** 640–643 (2017).